Proceedings World Geothermal Congress 2010
Bali, Indonesia, 25-29 April 2010

Fracture Characterization and Stochastic Modeling of the Granitic Basement in the HDR Soultz Project (France)

Benoît Massart[1], Marie Paillet[1], Vincent Henrion[1], Judith Sausse[2], Chrystel Dezayes[3], Albert Genter[4], Adrien Bisset[5]

[1] CRPG-CNRS, ENSG, Nancy Université, rue du doyen Marcel Roubault, BP 40, 54501 Vandoeuvre-lès-Nancy, France
[2] Nancy Université, Département des Sciences de la Terre, UMR CNRS 7566 G2R, BP239, 54506 Vandoeuvre les Nancy, France.
[3] Département Géothermie, BRGM, 3, avenue C. Guillemin - BP 6009 - 45060 Orléans Cedex 2, France
[4] EEIG Exploitation Minière de la Chaleur, Route de Soultz, BP38, F-67250 Kutzenhausen, France
[5] BeicipFranlab, 232, Av. Napoléon Bonaparte, 92502 Rueil-Malmaison, France

Keywords: Fractures, faults, statistics, Soultz, damage zone, fractal dimension, Discrete Fracture Networks

ABSTRACT

The quantification and modeling of fluid flow in fractured rocks are extensively studied to solve and predict numerous economic and environmental problems (hydrothermalism, geothermy, storage, etc.). Discontinuities such as faults and fractures are potential sites for fluid circulation and have important implications on the hydraulic properties of rocks. The matrix permeability of igneous rocks is generally small and, consequently, the global permeability is mostly controlled by the fault and fracture networks. Therefore, the quantification of the fractured rock hydraulic properties strongly depends on the knowledge of the geometrical parameters of the fractures (orientation, extension, aperture, density) and of the final 3D modeling of the fracture network organization.

In the specific case of the Soultz-Sous-Forêts geothermal reservoir, a new method of statistical analysis of fault and fracture networks is proposed to accurately model the actual 3D structure of the reservoir (Sausse et al., 2009; Dezayes et al., 2009). The statistical characterization of the fractures and faults was realized via reinterpretation of the entire database of U.B.I. images available at Soultz. 1800 fractures were determined along the three deep Soultz well paths and grouped into main conjugate fractures sets. These fractures have a mean N-S orientation and a mean dip of 70°, which is consistent with the Oligocene N-S extension responsible for the formation of the French Rhine graben. A power-law type correlation between the geometric parameters of fractures is proposed in Equation 1:

$$L = k \bullet W^{D} \quad (1)$$

where W and L are fracture width and length, respectively, k is the coefficient characteristic of the facies, and D is the fractal dimension of the fracture set. These parameters were used to determine the volumetric density of fractures (number of fractures/m^3) at the well scale. Finally, this density and the statistics of fracture properties were used to constrain stochastic simulations of a discrete fracture network (DFN) in the geothermal reservoir.

1. INTRODUCTION

The geothermal reservoir of Soultz-Sous-Forêts is a naturally fractured granitic basement located in the Rhine graben in Alsace, France, where a thermal anomaly of around 200°C has been observed at a depth of 5000 m. Soultz was implemented in 1987 as the site for a European experimental geothermal pilot plant because of its high temperature at depth and the locations of other oil-producing wells in the historic Pechelbronn field region, which provide much information concerning the geology of the basin. High pressure water is injected into non-porous but fractured media in order to stimulate the natural existing fractures in the rock via hydraulic fracturation. This enhances the fracture permeability and connectivity between the injection and production wells and within the reservoir. A geothermal triplet configuration is employed, in which cold water is injected in a central well and is produced from two other lateral wells after being heated at depth.

In this case, the fracture network mainly controls the hydraulic behavior of the reservoir. Thus, the characterization of fractures is crucial for the study of flows and for production optimization. This analysis is reliable on the well scale where Ultra Sonic Borehole Images (U.B.I.) data are available, but there is a large degree of uncertainty on the reservoir scale far from the wells. Moreover, in the case of basement fractured rock such as those at Soultz, fractures and faults represent complex and composite structures. A fault zone is characterized by a large damage zone where intense microfracturing and alteration may be observed (Genter et al. 2000). These complex fault zones constitute the main drains of the reservoir.

A new statistical interpretation of the fracture and faults at Soultz is presented in this work. The characterization of the main fracture sets allowed the modeling of a DFN (Discrete Fracture Network) in the reservoir and the derived hydraulic properties, which were compared to the results of the numerous flow tests performed at Soultz. The focus of this paper is on the different steps of statistical analysis and determination of the set parameters of the fractures. The chosen criteria that constrained the DFN simulation are also proposed. The objective of this study is to construct a consistent DFN model that can be used as a basis for flow study.

2. GEOLOGICAL DATA: ACQUISITION AND PROCESSING

Soultz-Sous-Forêts, located in the Upper Rhine Graben, hosts one of the few deep geothermal 'Enhanced Geothermal System' test sites in the world. At its current state of development, the EGS site consists of six boreholes (Gérard et al. 2006). GPK2, GPK3 and GPK4 constitute the European geothermal pilot plant which extends to more than 5000 m depth. GPK1 is the first hydraulic test well and extends to 3600 m. EPS1 is a reference hole which has been fully cored down to 2230 m. Some seismic observation wells are located near the geothermal plant, of which Well 4550 is the closest to the wellhead of GPK1. The configuration of Wells GPK1 – GPK4 and EPS1 are shown in the diagram in Figure 1A.

The French Geological Survey (BRGM) collected geological and well logging data to characterize the Soultz fractured

granite reservoir in terms of petrography, hydrothermal alteration and natural fracture network. Well data were acquired by logging companies. Numerous hydraulic stimulations of the deep wells induced micro-seismic activity, which was interpreted in terms of major structures in order to relate event locations with fault organization (Dorbath et al, in press). Numerous hydraulic data such as flow logs are also available (Nami et al., 2008, Schindler et al., 2008).

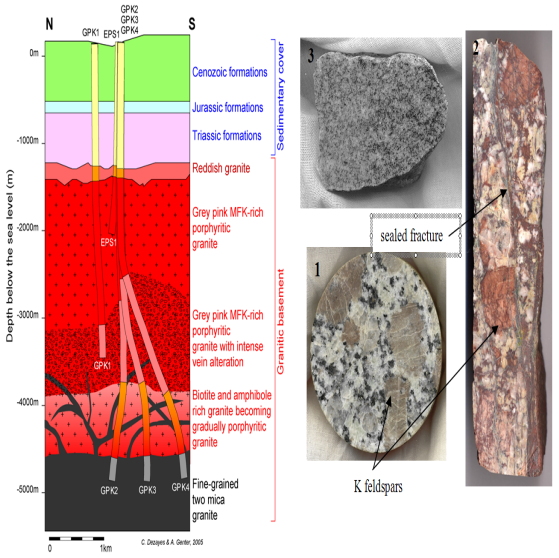

Figure 1: A. Lithological schematical cross-section of the Soultz site (Dezayes et al. 2005). B. Picture 1 : plug of the fresh porphyritic granite facies (well GPK1(K5-20)); Picture 2 : strongly altered porphyritic granite facies, one sealed fracture could be observed (well GPK1, K21, 3510 m); Picture 3 : Two-mica granite facies (well GPK2, K1, 5058.30 m).

2.1. Facies of the Soultz Granite Reservoir

The Soultz basement is represented by two different facies. The first is a monzogranite facies observed under Triassic to actual sedimentary deposits at a 1200 m depth and consists of porphyritic granite. This granite is rich in potassic feldspars appearing in a quartz, plagioclase, biotite and amphibole matrix. This first facies could be significantly altered locally, as shown in Picture 1 in Figure 1.B. (Genter 1989). This intense alteration is caused by a succession of hydrothermal events of three types:

- A generalized and pervasive alteration of the matrix by formation water flows.
- An illitization localized in the fracture zones, which matches the high Gamma-Ray signatures on geophysical well logs. This alteration leads to the sealing of the majority of natural fractures, which depletes permeability almost completely. (See Figure 1.B., Picture 2.)
- A rubefaction of the top of the granite due to its emersion and its alteration by surface waters.

The second facies, which is crosscut by the wells at high depth (> 4000 m), is a two-mica facies composed of biotite and muscovite in a grey quartz matrix. The facies is more homogeneous and less affecte by the hydraulic alteration than the upper one, as can be seen in Figure 1B, Picture 3 (Dezayes et al. 2005).

2.2. Faults and Associated Damage Zone

In the case of the Soultz reservoir modeling, particular attention was paid to the modeling of the faults. Dezayes et al. (2009) and Sausse et al. (2009) recently proposed a new 3D model of the fault networks based on high quality datasets including geological data, well logs, microseismicity recordings during hydraulic stimulations of the wells, and vertical seismic profiling (V.S.P.). One major fault is identified in GPK1, GPK2 and GPK3 where the majority of the fluid losses during flow tests is concentrated (75 % of fluid loss). This major fault represents a complex clustered structure when observed at well scale and appears with a large damage zone on U.B.I. images. A damage zone consists of a volume of deformed rocks around a fault surface that results from the initiation, propagation, interaction, and buildup of slipping along faults (Kim et al. 2004). The resulting displacement is balanced by the opening of conjugate fractures along the fault plane. The damage zone becomes larger with fault growth. The first initial fractures grow simultaneously and in turn generate fractures to balance their opening. Genter et al. (2000) proposed a damage zone model of the fracture zones observed at Soultz. Three zones could be identified from the fault core to its periphery, as illustrated in Figure 2:

1. The fault core is the least porous part of the damage zone. In this example, it is mainly sealed by secondary quartz crystallization.
2. The cataclased and brecciated zones are more or less obstructed by fine particles, shales, or silts, which are generated by the shear along the fault.
3. The hydrothermally altered zones are high porosity zones where fluids flows are likely concentrated.

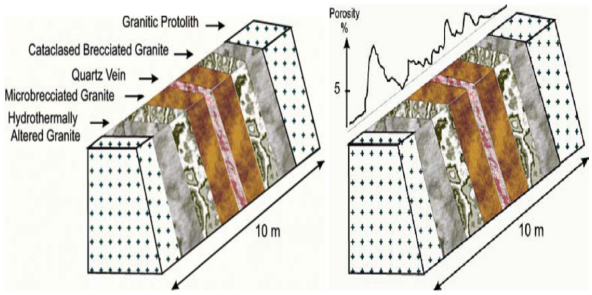

Figure 2: Conceptual lithofacies granite zonation and porosity profile of a hydrothermally altered and fractured zone at Soultz (Genter et al. 2000).

The major fault observed in GPK3 generated a damage zone about 13 m wide along the well path.

3. STATISTICAL ANALYSIS OF ULTRASONIC BOREHOLE IMAGES (U.B.I.)

3.1. Ultrasonic Borehole Imagery (U.B.I.) and Fracture Identification

Wells GPK2, GPK3 and GPK4 were logged with U.B.I. tools. These acoustic tools record amplitude and transit time data of acoustic waves reflected by the borehole walls and therefore allow the determination of contrast of sonic velocities that reveal facies variations of the fracture zones, as illustrated in Figure 3A.

Centimetric fractures could be detected thanks to the accurate U.B.I. vertical resolution of 0.5 – 1 cm. However, the sonic wave lateral penetration is quite low, with a sampling interval of 0.1 inches (2.54 mm).

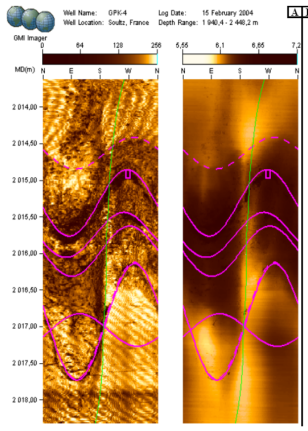

Label	Fracture type
1	Discontinuous open
	0-25 % of the UBI trace
2	Discontinuous open
	25-50 % of the UBI trace
3	Discontinuous open
	50-75 % of the UBI trace
4	Vuggy fractures
5	Continuous open
	Fine aperture, more than 75 % of the UBI trace
6	Wide open
	Big aperture, more than 75 % of the UBI trace
7	Damage zones
	Intensed fractured zones
8	Horizontal induced fractures
9	Vertical induced fractures

Figure 3: A. Examples of fracture and damage zone identifications in U.B.I. images. The pink sinusoidal curves correspond to fracture traces, which in turn corresponding to contrasted amplitudes (left U.B.I. image) and transit times (right U.B.I. image). An open fracture is characterized by both amplitude and transit time traces. The dotted curves mark the boundaries of damage zones. The true dip and dip direction of the fractures are derived from the sinusoidal curve characteristics. B. Selection and classification of the fractures.

The sole focus of this work is the open fractures that host fluid flow in the reservoir. However, the actual effective opening of a fracture remains difficult to define. Closed fractures are sealed by secondary re-crystallization or filled with fine impermeable particles (only amplitude traces on U.B.I.). The main faults present damage zones and largely open fractures (both amplitude and transit time traces on U.B.I.). Between these two extreme opening states, several other degrees of fracture width are proposed in this study and listed in Figure 3B.

A total of 1878 open fractures were located on GPK2, GPK3 and GPK4 UBI logs, as shown in Figure 3.B. 1637 of these fractures were defined as natural open fractures (labels 1 to 6), 82 were defined as damage zones (label 7), and 159 were defined as horizontal induced drilling fractures (label 8). The measured depth, true dip, dip direction, and aperture (continuous or fragmented sinusoids) of each fracture were recorded.

Other previously occurring main fracture zones were characterized by labels 11 – 14 (Sausse et al., 2009; Dezayes et al., 2009).

3.2 Statistical Analysis of Fractures versus Labels, Orientations and Facies

The main results of the fracture database statistical analysis are presented in Table 1.

Fractures of the three deep wells GPK2, GPK3 and GPK4 are organized in two main orientations sets showing a mean North-South direction and East or West dips forming conjugated sets coherent with the direction of the Rhine Graben opening. Thus, the statistical analysis of each orientation set was performed, with 'Fracture set W' indicating the West dipping fractures and 'Fracture set E.' indicating the East dipping ones. The Fisher coefficient was determined for each set. This parameter is equivalent to the standard deviation parameter in the case of spherical geometry space such as orientation data. Low Fisher coefficient values indicate a high dispersion of orientations within a set, and high values indicate homogeneous or well distributed orientations. In this case, the Fisher coefficients ranged from 0.6 – 10.68. The same order of magnitude is observed for sets W and E, with lower dispersion for the dips than for the dip directions, as can be seen in Table 1.B and 1.C.

Table 1: Main results of the fracture database statistical analysis. A. The number of fractures and their relative proportions are presented according to facies and orientation sets. B & C. The mean dip directions, dips and, linear densities along the well paths for the two main sets: West (B) and East dips (C).

A	Label & fracture type	Number of fractures	rate (%)	Number of fractures FACIES 1	Number of fractures FACIES 2	Number of fractures SET W	Number of fractures SET E
1	Discontinuous open traces (25%)	1361	72.47	1170	191	837	524
2	Discontinuous open traces (50%)	85	4.53	83	2	47	38
3	Discontinuous open traces (75%)	30	1.60	21	9	16	14
4	Vuggy Fractures	125	6.84	117	8	86	39
5	Continous open	23	1.22	20	3	17	6
6	Wide open	13	0.69	10	3	8	5
7	Damage zones	82	4.37	80	2	49	33
8	Induced subhorizontal drilling fractures	159	8.47	137	22	88	71
	Total	***1878***	***100***	***1638***	***240***	***1148***	***730***
	Fracture density (Fractures/m)			***1.890***	***0.952***	***0.18***	***0.12***

		SET W				
B	Label & fracture type	Mean Dip Direction	Fisher coefficient	Mean Dip	Fisher coefficient	Fracture density (Fractures/m)
1	Discontinuous open traces (25%)	263	0.73	68	5.8	0.202
2	Discontinuous open traces (50%)	249	0.92	67	5.65	0.177
3	Discontinuous open traces (75%)	246	1.3	61	3.74	0.003
4	Vuggy Fractures	270	0.6	63	4.77	0.017
5	Continous open	247	1.29	72	8.24	0.006
6	Wide open	241	1.14	58	10.68	0.002
	All fractures	266	0.72	68	5.57	***0.18***

		SET E				
C	Label & fracture type	Mean Dip Direction	Fisher coefficient	Mean Dip	Fisher coefficient	Fracture density (Fractures/m)
1	Discontinuous open traces (25%)	81	1.1	69	5.57	0.134
2	Discontinuous open traces (50%)	77	1	74	10.07	0.012
3	Discontinuous open traces (75%)	96	1.23	70	6.87	0.004
4	Vuggy Fractures	74	1.17	71	7.32	0.011
5	Continous open	76	3.89	71	10.68	0.002
6	Wide open	117	1	71	2.71	0.002
	All fractures	77	1.06	70	5.65	***0.12***

The linear fracture density was calculated using the ratio of the number of fractures observed on U.B.I. logs to the total logged length of the well path. Global fracture densities (Sets W and E) of 1.890 and 0.952 fractures/m were observed in facies 1 and 2, respectively. This difference could be explained by the different mechanical behaviors of the granitic facies and the resulting types of fracturing. The two-mica facies could have a more plastic behavior due to the high occurrence of anistropic micas.

Discontinuous open fractures are the most numerous: labels 1, 2 and 3 represent 78.6% of the entire fracture database. This fracture type is more represented in the two-mica granite facies than in the porphyritic granite facies. The two-mica granite shows less alteration and less numerous fractures than the porphyritic granite. Only a few vuggy, continuous and wide open fractures have been observed (8.5% of the whole database). These fractures that represent the main drains in the reservoir and remain isolated in the largest structures described by Dezayes et al. (2009) and Sausse et al. (2009).

The conjugated sets are not distributed homogeneously with depth. The first facies hosts a higher rate of West dipping fractures (60%) than East dipping fractures (40%). The bottom part of the reservoir in the second facies shows a majority of West dipping fractures (80%). The in-situ stress tensor and the resulting fracture orientations at depth could be modified due to the presence of big faults of the Rhine graben (Dezayes et al. 2009).

3.3. Statistical Analysis of Fracture Sizes and Widths

D.F.N. (Discrete Fracture Network) modeling of the fractured reservoir requires the definition of the volume of interest (V.O.I.) around the reservoir wells, which is represented by a regular grid containing voxels characterized by a volumetric fracture density property. The fracture database is acquired at the well scale. However, the major issue in reconstructing the 3D geometry of the Soultz fracture network is the question of the fracture extensions.

The extension of a fracture is linked to its width according to Equation 1 (Johnston, 1996).

3.3.1 Fractal Dimension of the Fracture Network

Mandelbrot (1984) defines a fractal object as a rough or fragmented geometric shape that can be split into identical parts, whatever the scale of observation. This property is called self-similarity. Each elementary shapes is (at least approximately) a reduced-size copy of the whole shape and has a probability of occurrence P that is related to the fractal dimension D according to Equation 2:

$$P = x^{-D} \qquad (2)$$

where x is the characteristic length of the shape that could be the extension of the fracture or its width. The fractal dimension D is a decimal number that ranges from $1-2$ in 2-D studies. Low D values indicate clustered events, while high D values correspond to more regularly spaced ones.

Two approaches were used to determine the fractal dimension of the Soultz fracture network. All approaches are described precisely by Bonnet et al. (2001):

- The first approach employs the frequency distribution of the fracture width.
- The second approach is the spacing interval method (Harris et al. 1991).

Frequency Distribution of the Fracture Geometry: Number of Fractures versus Mean Width per Label

The new fracture database presented in this paper includes all fracture types, faults and damage zones observed in Wells GPK2, GPK3 and GPK4 and was analyzed according to the relationship between fracture occurrences (probability of fracture intersection with the wells) and widths, as proposed by Bonnet et al. (2001). The damage zones do not strictly represent fractures, but their vertical extension along the wells was assimilated to the width of the associated faults previously defined by Dezayes et al. (2009) and Sausse et al. (2009). For example, the major fault that intercepts Well GPK3 at 4775 m (M.D.) is surrounded by a damage zone of 13 m. This fault is therefore characterized by a 13 m width equal to its damage zone width in the database. A bi-logarithm diagram is presented in Figure 4, in which the number of fractures n of each label is plotted as a function of their mean width W. White dots in Figure 4 correspond to the fracture labels correlated over a large magnitude of fracture widths. Black dots are "problematic" plot points, corresponding to fracture labels 5 and 6. This relation is well fit (R^2=0.9665) to a power law equation with an exponent equal to 1.04.

A

	Label & fracture type	Mean widths W (cm)	Number of fractures
1	Discontinuous open traces (25%)	3.15	1476
2	Discontinuous open traces (50%)		
3	Discontinuous open traces (75%)		
4	Vuggy Fractures	10.69	125
5	Continous open fractures	6.32	23
6	Wide open fractures	20.31	13
11	minor faults	150.11	18
12	medium faults	269.83	8
14	major faults	626.53	4

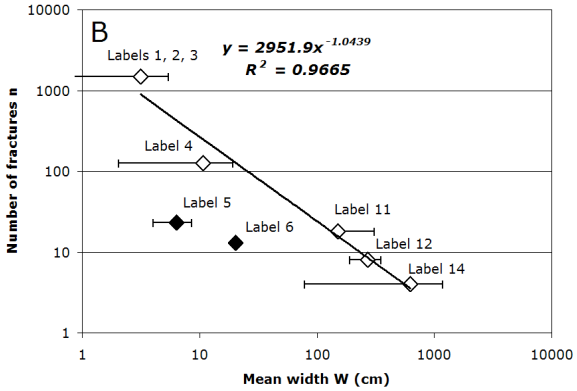

Figure 4: A. Data used for the each fracture label plot. The values in brackets correspond to extrapolated data, proportional to the number of fractures. Labels 5 and 6 were not correlated to the general trend and were removed from the database for the calculation of the cumulative probability. Labels 11, 12 and 14 correspond to faults with damage zones located on U.B.I. images. Labels 11 and 12 correspond to the smallest and medium faults, respectively (in term of fracture size). Label 14 corresponds to the main fault of the Soultz reservoir. B. Bi-logarithm diagram representing the number of fractures *n* as a function of their width *W* (cm).

The general trend observed in Figure 4 was not adapted to describe fracture labels 5 or 6, which represent continuous or wide open fractures in the U.B.I. images. These fractures are not sufficiently numerous to fit the general trend. One possible explanation is that only open fractures were taken into account in this study. Indeed, many fractures of the same types are at present completely sealed by sequences of

hydrothermal alteration. These sealed fractures were formed at the same time as those described by labels 5 and 6 and are still open today. The paleo-fractures have similar widths to the open fractures, but they are sealed widths. These wide and continuous open fractures are the main fractures that could be penetrated within the rock mass, insuring the pervasive alteration of the granite, while large faults cause more localized vein alteration (Sausse and Genter, 2006). Thus, one possible explanation of this underestimation of the number of label 5 and 6 fractures is that the missing label 5 and 6 fractures are now sealed and therefore not taken into account in the database.

Fracture labels 1, 2 and 3 are merged in a single group in the plot in Figure 4 because of the huge proportion of label 1 fractures in the database that mask the influence of 50% and 75% of continuous fracture traces. This distinction is therefore not discriminant in this study.

The low fractal dimension of 1.04 indicates that fractures are strongly clustered. This organization of very dense fracture zones around the main fault corridors is well known at Soultz (Sausse and Genter, 2006).

Cumulative number of fractures versus width

Harris et al. (1991) proposed to plot the cumulative number of fractures N_S as a function of their mean spacing S in a bi-logarithmic diagram, where N_S is the number of fracture spacing values higher than a specific spacing S. This plot is shown in Figure 5.

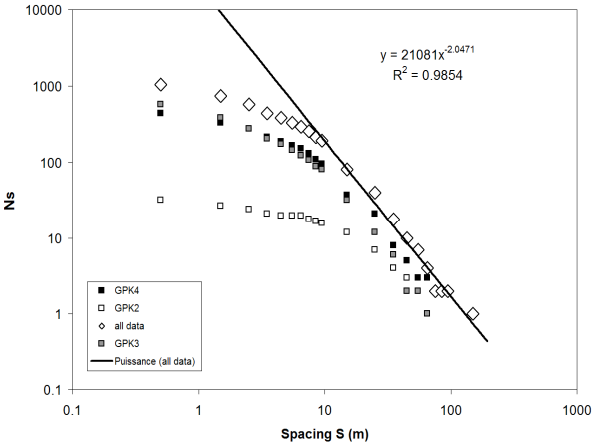

Figure 5: Bi-logarithmic diagram of the cumulative number of fractures N_s as a function of their spacing S. A line is the best-fit curve of the entire fracture spacing database. The power law follows the equation $N_s \sim S^{-(D+1)}$ where D is the fractal dimension characterizing the fracture set.

The spacing S is the mean of the distances along the well path between one fracture and fractures i-1 and i+1. This methodology has been applied to each Soultz deep well (GPK2, GPK3 and GPK4) and the three resulting plots were compared. Harris et al. (1991) proposed a relation between N_s and S following Equation 3:

$$N_s \approx S^{-(D+1)} \quad (3)$$

where D is the fractal dimension of the fracture set. The best-fit curve following Equation 3 is quite difficult to determine in this case because of the dispersion of N_s and S. However, the same fractal dimension D of 1.04 was obtained and corresponds to a curve slope s of -2.04. A D-value of 1.04 ± 0.1 (i.e. D in [1;1.1]) seemed to be well adapted to describing the spacing data (R=0.8701) of the three Soultz wells.

3.3.2 Extension of the Fractures

Determining the extension of a fracture is the main source of uncertainty in the hydraulic models. In fact, there is no consensus between authors concerning the best and most relevant method.

Gundmusson (2000) made observations at the reservoir scale concerning the length of veins observed in flow lavas. He determined that there is a linear relationship between the extension of a fracture L and its width W, as shown in Equation 4 :

$$L = k \cdot W \quad (4)$$

where k is a coefficient characteristic of the facies. In the case of the veins observed in flow lavas, k is equal to 400 but has a poor correlation factor of R = 0.81.

Vermilye and Scholz (1995) state the same observations on fractures in different magmatic and sedimentary facies. In the case of the granodiorite of the Florence Lake, quite similar to the monzogranite of Soultz (porphyritic granite), the coefficient k is equal to 526 with a good correlation factor of R^2 = 0.96 (42 measurements with extensions ranging from 23 mm to 23.7 m and widths ranging from 0.1 mm to 4.5 mm). However, the authors noticed that the correlation factors are sometimes very poor for linear regression (R^2 = 0.28 in limestones, R^2 = 0.22 in argilites, R^2 = 0.66 in sandstones).

Johnston (1996) proposed another relationship between width and extension. After collecting data for five study areas with widely varying structural geometries in a variety of host rock types, they determined that the extension and the width of a fracture are proportional in some cases, but that they follow a more generalized power-law of the form given in Equation 1, where the coefficient characteristic k ranges from 20 – 2000 for granitic facies. The coefficient k is higher in extensional context than in a context of compression, ranging from 57 – 1231, with a mean value of 402.

It was decided to follow the hypothesis of Johnston (1996) the mean extension of the different labels was calculated using values of $k = 400$ and $D = 1.04$. The results are reported in Table 2.

Table 2: Mean fracture extension by fracture labels

Label & fracture type		Mean widths W (cm)	Mean extensions L (m)
1	Discontinuous open traces (25%)	3.15	11
2	Discontinuous open traces (50%)		
3	Discontinuous open traces (75%)		
4	Vuggy Fractures	10.69	39
5	Continous open fractures	6.32	23
6	Wide open fractures	20.31	76
11	minor faults	150.11	610
12	medium faults	269.83	1123
14	major faults	626.53	2697

The width of the damage zone associated to the major fault at Soultz is equal to 13 m. By application of Equation 1, its extension was found to be 2.7 km. This could be an accurate estimation, because this fault crosses the three wells at a minimum distance of 2 km.

4. MODELING OF THE FRACTURES SET

4.1 Density of Fractures

To obtain the volumetric density of fractures (fractures/m^3), a method described by Chilès (personal communication), inspired by the work of Fouche and Diebolt (2004) was applied. First, the length L of the window in which the density was calculated was determined. A length of $L = 30$ m (resolution of the final VOI grid) was fixed. This window length was then moved along the wells meter by meter. For each window, the number of fractures n that crossed the well was determined. Then, for each window, the surface density $\tilde{A}_v$, which is the ratio of the surface of fractures that cross the well in the window to the volume of the window, was calculated. The assumption (H) that each fracture i fully contributed to the 3D density measured was proposed. After simplification, the surface density could be expressed using Equation 5:

$$\tilde{A}_v = \frac{1}{L} \cdot \sum_{i=1}^{n} \frac{1}{\cos\theta_i} \quad (5)$$

where θ_i is the true dip of fracture i.

This value of the surface density is overestimated because of the assumption (H). Fouche and Diebolt (2004) proposed the correction parameter F_n, which takes the Terzaghi correction into account for 2-D studies. The true surface density A_v was then expressed according to Equations 6 and 7:

$$A_v = F_n \cdot \tilde{A}_v \quad (6)$$

$$With\ F_n = \frac{n^2}{\sum_{i=1}^{n} \cos\theta_i \cdot \sum_{i=1}^{n} \frac{1}{\cos\theta_i}} \quad (7)$$

The next step was to determine the mean surface of a fracture in the window. The results of the statistical analysis that determined the extension L of each fracture as a function of its width W (Equation 1) with k = 400 and D = 1.04 were used. Fractures were described by disks with surfaces equal to $\pi(L/2)^2$. Finally, the volumetric density of fractures (fractures/m^3) was obtained by dividing A_v by S. This method was applied to Wells GPK2, GPK3 and GPK4, and the volumetric density is plotted for each well in Figure 7 using a true vertical depth reference (T.V.D.S.S.). Matching depth to location of the main faults that cross the wells and their associated damage zones is superimposed for GPK3 as an example.

Well GPK3 is the most fractured, with a mean density of 0.0056 fractures/m^3 (GPK2: 0.0015 fractures/m^3; GPK4: 0.0052 fractures/m^3). Well GPK4 is slightly less fractured than GPK3, but the difference between these two wells results from the distribution of fracture length. GPK4 showed the smallest fracture extensions despite having a quite similar volumetric density. This could explain its poor connectivity within the geothermic triplet.

Moreover, the influence of the faults and the extension of the damage zone can be observed clearly in Figure 7. The fracture density around the main faults (ZF, Labels 11, 12 and 14 in Figure 7) is systematically and artificially low in U.B.I. images because of the impossibility of practical fracture picking in the damage zones that show too high a density of thin fractures to clearly discern them. Grey zones in Figure 7 illustrate the density distribution around the main faults. The density peaks are symmetrical from fault walls and allow the definition of a fault "zone of influence" around their characteristic depth. This "zone of influence" is estimated for the largest fault zone (ZF-GPK3 Label 14 on Figure 7) at 200 m wide (above and below the main fault core). Other zones of influence could be clearly defined as showing lower amplitudes than this one.

Some correlation of density peaks could also be observed and must now be checked more precisely with the main fault orientations.

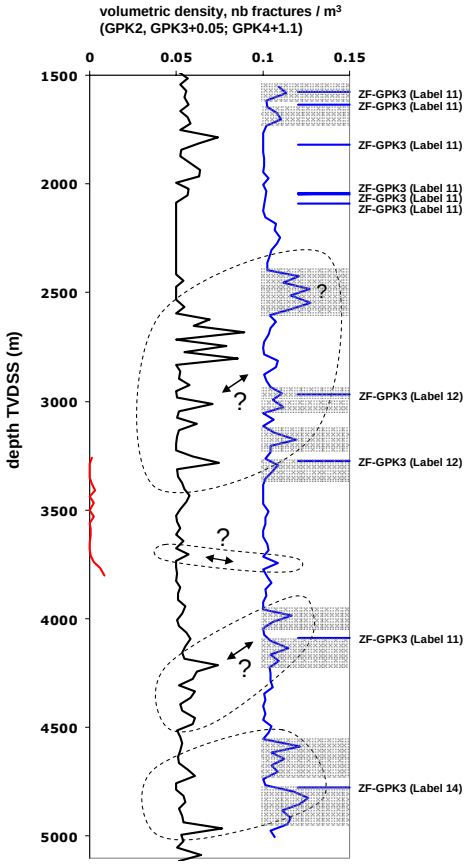

Figure 6: Volumetric density at Wells GPK2, GPK3 and GPK4. The curves corresponding to the wells GPK3 and GPK2 were shifted by the addition of 0.1 to the density of GPK3 and 0.2 to the density of GPK4.

4.2 Stochastic Modelling

The statistical analysis and calculation of the volumetric density of each well allowed the initiation of the simulation process of the first DFN model. A D.F.N. process generates fractures as points distributed in the reservoir using a Poisson point process. Each fracture is characterized by its center and two vectors: its orientation (dip direction and dip) and its extension. These parameters are defined by distribution laws, whose characteristics are defined by the previous statistical analysis. Thus, the distribution of the extension is not Gaussian, but it follows a power-law distribution. The extension is defined according to Equation 1 ($L = k\,W^D$), and the fracture occurrence is defined according to Equation 2 ($P = k'\,W^{-D}$).

The fracture extension distribution follows a power-law distribution and is the same as those observed for the different fracture labels. The dip directions and dips follow Gaussian distributions that are defined for each facies and fracture set using mean values and standard deviations or

Fisher coefficients. The parameters of extension, dip direction, and dip were assigned to the simulated points using the Monte-Carlo process.

The preliminary results of such D.F.N are currently being realized. The difference between the fracture densities of the two granite facies was considered, and the difference of fracturing is visible. Such types of D.F.N. allow the calculation of the equivalent porosity and permeability properties in the VOI grid. Initial results yielded mean values of porosity around 5% and permeability around 25 milliDarcy in the reservoir. These initial results must now be matched with the characteristic flow logs obtained since 2000 for GPK2, GPK3 and GPK4.

5. CONCLUSIONS

A new method of statistical analysis of the fault and fracture networks of the Soultz reservoir was used to model the structure of the reservoir. The statistical characterization of the fractures using U.B.I. images allowed the definition of 1800 fractures along the three deep Soultz well paths. These fractures were grouped into main conjugates fractures sets, showing a mean N.-S. orientation and a mean dip of 70°. Power-law type correlations between geometric parameters of fractures (aperture, width and size) were determined, and a final fractal dimension *D* characterizing the fracture set was proposed. These parameters were used to determinate the volumetric density of fractures at the well scales and then within the reservoir grid. Finally, the results of statistical analysis were used to perform the stochastic simulation of a Discrete Fracture Network (D.F.N.). The comparison of D.F.N. reservoir models to flow test results must be performed in order to define the uncertainties concerning the adjustment of the density maps, the influence of the various parameters (extensions, orientation distributions, etc.), and their impact on the hydraulic modeling of the reservoir.

REFERENCES

Bonnet, E., Bour, O., Odling, N., Davy, P., Main, I., Cowie, P., and Berkowitz, B.: Scaling of fracture systems in geological media. Geophysics, 39, (2001), 347-383.

Dezayes, C., Chevremont, P., Tourliere, B., Homeier, G., and G. André.: Geological study of the GPK4 HFR borehole and correlation with the GPK3 borehole (Soultz-Sous-Forêts, France). Technical Report RP-53697-FR, BRGM, France, (2005).

Dezayes, C., Genter, A., and Valley, B.: Structure of the low permeable naturally fractured geothermal reservoir at Soultz, Geosciences, (in press), (2009).

Fouché, O., and Diebolt, J.: Describing the geometry of 3D fractures systems by correcting for linear sampling bias. Mathematical Geology, 36, (2004), 33-63.

Genter, A.: Géothermie Roches Chaudes Sèches: le granite de Soultz-Sous-Forêts (Bas Rhin, France). Fracturation naturelle, altérations hydrothermales et interactions eau-roche, PhD thesis, Orléans University, BRGM, (1989), 201 p.

Genter, A., Traineau, H., Ledésert, B., Bourgine, B., and Gentier, S.: Over 10 years of geological investigations within the HDR Soultz project, France. Proceedings, World Geothermal Congress 2000, Kyushu-Tohoku, Japan, May 28 - June 10 (2000).

Gerard, A., Genter, A., Kohl, T., Lutz, P., Rose, P., and Rummel, F.: The deep EGS (Enhanced Geothermal System) project at Soultz-Sous-Forêts (Alsace, France). Geothermics, 35, (2006), 473-483

Gundmusson, A.: Fracture dimensions, displacements and fluid transport. Journal of Structural Geology, 22 (2000), 1221-1331.

Harris, C., Franssen, R., and Loosveld R.: Fractal analysis of fractures in rocks: the Cantor's dust method - comment. Tectonophysics, 198 (1991), 107-115.

Johnston, J.-D., and Mc Cafrey, K.: Fractal geometries of vein systems and the variation of scaling relationships with mechanism. Journal of Structural Geology, 18, (1996), 349-358.

Kim, Y., Peacock, D., and Sanderson, D.: Fault damage zones. Journal of Structural Geology, 26 (2004), 503-517.

Mandelbrot, B.: Les objets fractals, forme, hasard et dimension. Nouvelle Bibliothèque Scientifique, 2nde édition, Flammarion, Paris, (1984).

Nami, P., Schellschmidt, R., Schindler, M., and Tischner, T.: Chemical Stimulation Operations for Reservoir Development of the Deep Crystalline HDR/EGS System at Soultz-Sous-Forêts (France), Proceedings, 33rd Workshop on Geothermal Reservoir Engineering, Stanford University, Stanford, California, January 28-30 (2008).

Sausse, J., and Genter, A.: Types of permeable fractures in granites, Special publication of the Geological Society of London (Harvey P.K., Brewer T.S., Pezard P.A. and Petrov V.A. (editors), 240 (2006), 1-14.

Sausse, J., Dezayes, C., Dorbath, L., Genter, A., and Place, J.: 3D model of fracture zones at Soultz based on geological data, image logs, induced microseismicity and vertical seismic profiles, Geosciences, (in press), (2009).

Schindler, M., Nami, P., Schellschmidt, R., Teza, D., and Tischner, T.: Review of Hydraulic Stimulation Operations in the 5 km Deep Crystalline HDR/EGS-Reservoir at Soultz-sous-Forêts, Proceedings, 33rd Workshop on Geothermal Reservoir Engineering, Stanford University, Stanford, California, January 28-30 (2008).

Vermilye, J., and Scholz, C.: Relation between vein length and aperture. Journal of Structural Geology, 17, (1995), 423-434.